

Theses of the PhD thesis

Artifact Reduction in Computed Tomography

Csaba Olasz

Supervisors:

László G. Varga, PhD, assistant professor

Antal Nagy, PhD, associate professor

**Doctoral School of Computer Science
University of Szeged**

Department of Image Processing and Computer Graphics

2024

1 Introduction

Computed Tomography (CT) is an imaging technique in which an object can be reconstructed slice-by-slice without damaging the object [13]. To achieve this, one exposes the object of study to some kind of penetrating wave or radiation (e.g., X-ray, seismic waves, ultrasound, neutron beams, radio waves, etc.) and uses mathematical tools to derive the structure of the object from the changes of the waves passing through the object or reflected from it [8]. CT has a wide scope of applications considering fields such as medical imaging [15], geology [10], non-destructive testing [14], etc.

In the case of transmission X-ray tomography, measurements are taken with penetrating X-ray radiation. As the radiation passes through the object, it attenuates proportionally to the linear attenuation coefficient of the material it crosses. There are multiple sensors placed behind the object, where the total attenuation of an X-ray beam is detected at a given view angle. One can reconstruct the attenuation coefficient at any given point of an object if a large enough number of measurements are available at different view angles.

Measurements used by a tomographic method are usually affected by distortions [9]. Many sources of distortions exist, among which the most common problems are physical phenomena related to data acquisition, such as beam hardening and Compton scattering. Measured values can also be affected by electrical noise [7], and geometric inconsistencies in the CT scanner can cause additional artifacts. Furthermore, the reconstruction method itself and the discrete representation of the resulting images may also introduce errors [8].

This thesis summarizes the research of the author in the field of transmission X-ray tomography. The binding concept of the conducted research was to improve the quality of the reconstructed image with the reduction of previously mentioned artifacts by improving existing reconstruction algorithms and the fusion of CT and Convolutional Neural Network (CNN) techniques.

The number of projections and detector elements in a CT is limited. In addition, reconstruction is usually performed on a discrete grid. These restrictions of the model create artifacts in the reconstructed images. In Chapter 2, I show that the type of interpolation used during forward projection and backprojection strongly influences these artifacts (i.e. *interpolation errors*). The connection between pixel coverage and interpolation error is also obtained to get a better understanding of the interpolation errors, and I also propose an effective correction method to reduce the effects of interpolation errors in reconstructed images. I tested the proposed method in a comprehensive experiment, where I found that the proposed correction method can significantly improve the quality of the reconstructed images.

Combining computer tomography with deep learning methods is an effective way to achieve improved image quality and artifact reduction in reconstructed images. In Chapter 3, I present three novel neural network architectures for tomographic reconstruction with reduced effects of beam hardening and electrical noise. In the case of two novel networks, multiple skip connections maintained a strong bound between the parts of the neural network that allowed the projection data and the reconstructed image to be improved together. The proposed methods were tested on datasets generated by me. The datasets contain physically correct simulated data and show strong signs of beam hardening and electrical noise. We also performed a numerical evaluation on the reconstructed images corrected by neural networks according to three error measurements. The experi-

mental results showed that the reconstruction step used at the end of the neural network or in skip connections in neural networks improves the quality of the reconstructions.

1.1 Fundamentals

Let the attenuation coefficients of the material in a two-dimensional cross-section is represented by the $f : \mathbb{R}^2 \rightarrow \mathbb{R}$ function. The projections of f can be obtained by the Radon transform as

$$[\mathcal{R}f](\alpha, t) = \int_{-\infty}^{\infty} f(t \cos(\alpha) - q \sin(\alpha), t \sin(\alpha) + q \cos(\alpha)) dq, \quad (1)$$

where the (α, t) pair determines a line in the two-dimensional space, by giving its direction and distance from the origin, respectively. Figure 1 illustrates an object and one of its projections using parallel beam geometry, where a projection consists of projection lines that have the same α directions. With Equation 1 the mathematical description of the reconstruction problem can be defined as finding an f' , such that $[\mathcal{R}f'](\alpha, t) = [\mathcal{R}f](\alpha, t)$, for all measured (α, t) projection lines.

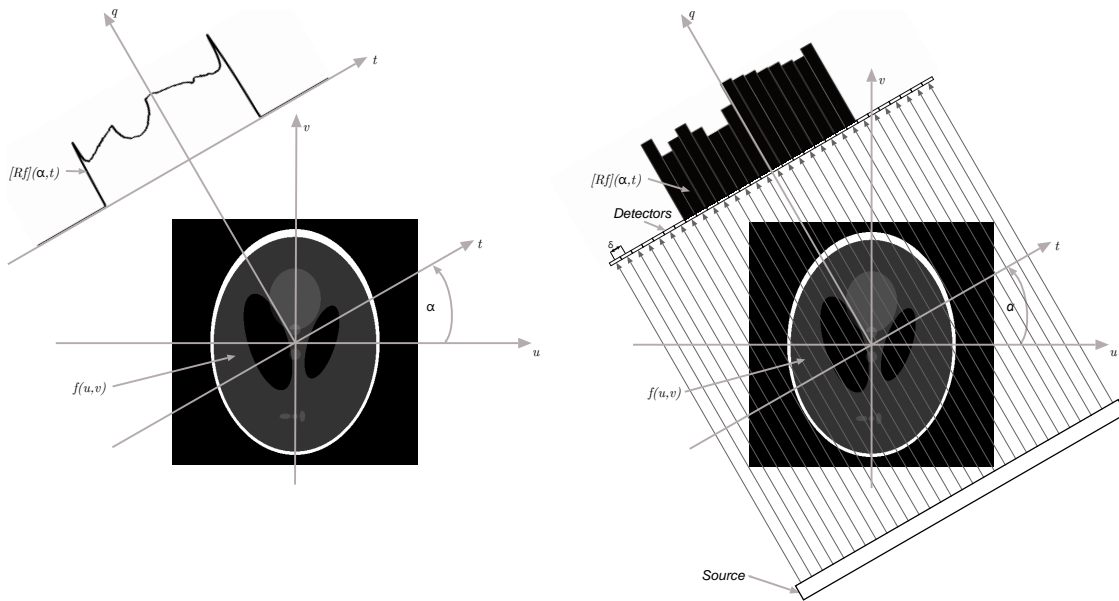


Figure 1: *Left, illustration of the Radon transform. Right, acquisition of a projection that highlights the discretized nature of the task.*

In CT scanners, the object of study is located between the X-ray source (S) and the detector (D), resulting in a limited span of f . Therefore, the range to be integrated can be simplified to the $[S, D]$ interval in Equation 1. We can say that the reconstruction of the object is performed on an $n \times n$ sized digital image consisting of uniform distinct pixels with sides of unit length. We also note that the measurements are available on a discrete grid due to the fact that the detector consists of multiple detector elements placed next to each other (see Figure 1).

With the above restrictions, we can define the reconstruction problem as a system of equations as follows: let us say, that we have an $n \times n$ image \mathbf{x} on a square grid indexed

in a row-major order, as shown in Figure 2. Furthermore, let the sinogram be a vector \mathbf{p} , with m_p projection angles each containing m_d detector values indexed in a detector-major order. In this way, let p_i ($i \in m$, $m = m_p \cdot m_d$) be the i -th ray shown in Figure 2. The following linear equation can be stated:

$$\sum_{j=1}^{n^2} W_{ij} x_j = p_i, \quad i = 1, 2, \dots, m, \quad (2)$$

where \mathbf{W} is the projection matrix (or system matrix), which contains the connection between all rays and pixels ordered by view angles. Basically, the W_{ij} is a weight that defines the x_j pixel proportion in the p_i projection.

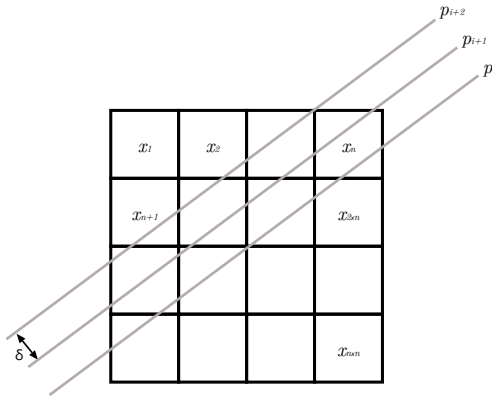


Figure 2: The reconstruction problem as a system of linear equations. x_n is the pixels of an image on a square grid. p_i is a ray at a given position and angle. δ represents the distance between neighboring rays.

2 Discretization artifacts

Real world objects have structures of infinite detail that one cannot capture technically and cannot handle computationally. Therefore, the reconstructed image and the projections are usually modeled on a discrete grid in transmission X-ray tomography. Due to the discrete representations, one can only give an approximate formulation of the projection geometry. Therefore, the weights of the projection matrix are calculated using the so-called “interpolation methods”. With the interpolation of the weights, one estimates the contribution of a certain pixel to the certain projection line. The different kinds of interpolation result in different structured artifacts in the reconstructed image. Figure 4 shows an example of an interpolation error by presenting the difference between the reconstructed image (*Raw*) and its ground truth (*GT*). The *GT* image is also presented. What we call interpolation error is the patterns originating from the center of the image and widening as the corners get closer.

Chapter 2 of the PhD thesis is built around the interpolation methods that I organized into two studies. In the *Comparison study*, I compared eight interpolation methods on our test dataset in multiple different settings. The included interpolation methods were *Cubic*, *MLinear*, *Nearest*, *Spline*, *Line*, *Linear*, *Strip* and *GDI*. After that, a correction technique is proposed in the *Correction Study* to reduce the errors caused by the interpolation methods.

2.1 Comparison study

Figure 3 shows the results in one of the multiple settings that I tested. Values are averages of the geometrical dataset using Structural Similarity (*SSIM*) [19] and 285 projections. The added noise levels indicated such as P is Poisson-type noise and G is Gaussian-type noise. The reconstructed algorithms tested were Filtered Backprojection (*FBP*) and the Simultaneous Iterative Reconstruction Technique (*SIRT*). The performance of the interpolation methods are different according to the *SSIM*. However, smaller differences can be obtained between the interpolation methods using *SIRT*. This suggest that the *SIRT* is less sensitive to the interpolation error than the *FBP*.

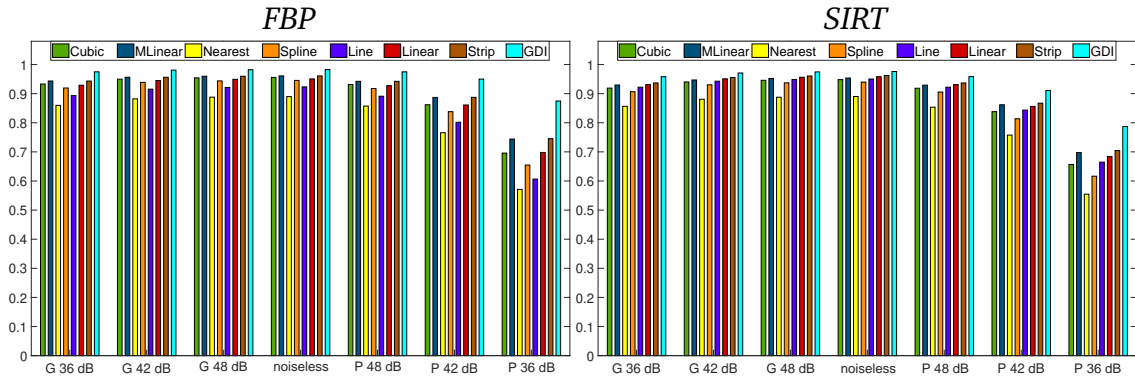


Figure 3: The diagrams show the average *SSIM* for the geometrical phantoms with 285 projections. The center of the diagrams shows the noiseless case. The effect of the Gaussain noise is shown to the left, Poisson noise to the right side.

2.2 Correction study

We found that the interpolation artifacts are diverse properties of the interpolation methods but are closely related to how much the rays contribute to a pixel in the projection geometry. The concept of obtaining the contribution is what we will call pixel coverage. It can be calculated in multiple ways by considering one ray or a group of rays. Let us define two versions of the pixel coverage using the notations introduced in (2). Let the global coverage of the j -th pixel of \mathbf{x} be defined as

$$\mathcal{C}_j = \sum_{i=1}^m W_{ij} , \quad (3)$$

giving the sum of coefficients in all the projections. Moreover, let Θ_k be the set of projection line indices i belonging to the projection angle k , and let the \mathcal{C}_{j,Θ_k} directed coverage of the j -th pixel be calculated as

$$\mathcal{C}_{j,\Theta_k} = \sum_{i \in \Theta_k} W_{ij} . \quad (4)$$

For each pixel this gives us the sum of projection coefficients within a projection.

The directed and global pixel coverage determine how much a pixel contributes to a projection or the sum of projections. It also reflects how much intensity is propagated into

the specific pixel when reconstructed. We assume that imbalances in the local and global pixel coverage show how uneven the representation of pixels in the geometry is, and thus can cause artifacts.

To show this phenomenon, we calculated projection matrices with the same geometries but different interpolations. We then calculated the global coverage of each x_j pixel for each interpolation. With *Line* interpolation, the resulting global coverage map is shown in the fourth row of Figure 4. Note that the global coverage map is what we will refer to simply as pixel coverage.

Our proposal is to even out the global coverage map by dividing the weights of the projection matrix in every given view angle by the corresponding directed coverage, i.e,

$$W'_{ij} = W_{ij} / C_{j, \Theta_k} \quad | \quad i \in \Theta_k \quad . \quad (5)$$

Basically, we normalize the weights by the sum of the weights within the angles. After normalization, the directed coverage map of W'_{ij} is equal to one for all angles. The effect of the correction is shown in Figure 4. Note that the patterns in the second and fourth column correlate with each other, and significant improvement was obtained after correction (third row) in the case of the *Line* interpolation.

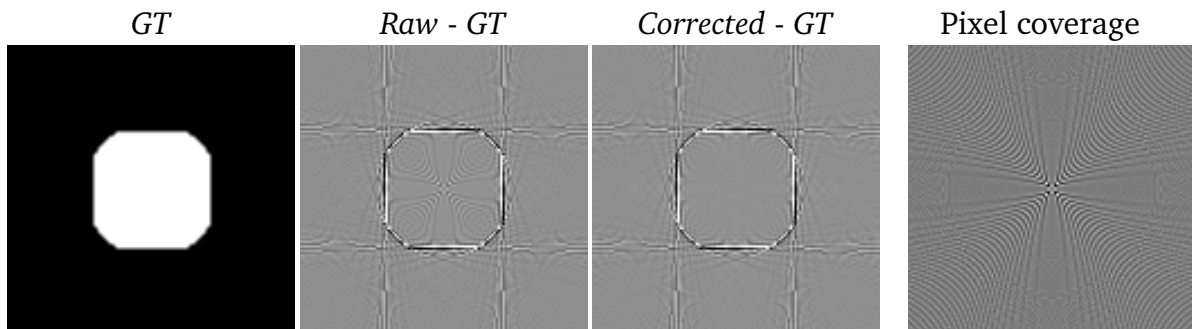


Figure 4: The ground truth (GT) phantom and the results with *Line* interpolation. *Raw*: reconstructed with the unnormalized projection matrix, *Corrected*: reconstructed with the normalized projection matrix and the global pixel coverage map.

3 Artifact reduction using U-net based neural networks

In one major topic of my research, I was working on combining the *FBP* with an outstandingly versatile and useful deep learning tool called U-net [17]. The U-net is an artificial neural network with a special structure, but generally speaking the U-net is part of the Convolutional Neural Network (CNN) [18] and deep learning [16] families as one of the sub-fields of artificial intelligence. These kinds of techniques have achieved outstandingly good results in the field of computer vision and digital image processing in the last decade. Similarly, the application of CNNs became a trend in CT research.

I present my work in Chapter 3 of this PhD thesis, where I combined the two fields in a unique way to provide highly accurate methods for the case of tomography when the projection data show strong signs of beam hardening and random electrical noise.

Beam hardening is a physical phenomenon [13], which occurs because the lower energy photons of the polychromatic radiation are absorbed with a higher probability in the material of the object studied than the higher energy photons. Therefore, if polychromatic radiation is passing through an object, it will lose a greater proportion of its lower energy photons, so the ratio of higher energy photons will increase relative to the lower energy photons. As this happens, one can say that the beam becomes harder, which means that the inner layers of the object will interact with radiation having a different characteristic. Beam hardening artifacts appear in two forms, such as cupping (the interior of the object appearing to be darker) and dark or light streaks (see Figures 5 and 6).

Another type of distortion that occurs during the data acquisition in tomography is called electrical noise. Electrical noise is a random factor in the measurement process causing random changes of the measured values [7]. In the reconstruction, it can cause streaks and random changes in the pixel values.

In order to cope with these distortions of the measurements (beam hardening and electrical noise) we introduce several changes to the original U-net structure [17]. Moreover, we designed three novel U-net based methods for reducing artifacts in the reconstructions. We needed a dataset to train neural networks; therefore we created a database with a virtual CT scanner called GATE [11, 12], producing realistic simulations of projection data.

3.1 FBP in the neural network

In this section we compare our neural network called *TomoNet1* with *DSENet*, *SinoNet* and *ReconNet*. All of these are based on the popular U-net structure, but their goal is different. The *DSENet* inputs are distorted projection data and its aim is to produce the error of the projection data in its output compared to ground truth projections. The *SinoNet* trained to improve the projection data as a preprocessing before the reconstruction step. On the contrary, *ReconNet* improves the reconstructed image after the reconstruction step. Our *TomoNet1* starts with *SinoNet* but we attached element after that corresponding to the *FBP* algorithm. In this way, the reconstruction step became part of the neural network.

The average (AVG) error and standard deviation (STD) of all test phantoms are shown in Table 1. We calculated three error metric namely the Peak Signal-to-Noise ratio (*PSNR*), Structural Similarity (*SSIM*) and Mean Squared Error (*MSE*).

Figure 5 displays the resulted images of the methods and the corresponding error maps. One can obtain a lot of streak artifacts with no correction, which are highlighted by the error maps. The error maps highlight the shape distorting effect of the *ReconNet*. Moreover, they confirm our observation on the inability of *DSENet* to decrease the electrical noise. The performance of the *SinoNet* and *TomoNet1* are similar looking at the error maps, but differences are visible in favor of the *TomoNet1*. Figure 6 shows the intensity profiles along the yellow lines of Figure 5.

3.2 Using FBP as skip connections in the modified U-net

In this section we introduced two novel neural network called *TomoNet2* and *TomoNet3*. In the case of these networks, multiple reconstruction layers were integrated into the structures as skip connections. These skip connections were able to maintain a strong bound

Table 1: The results of Section 3.1.

Method	No correction		DSENet		SinoNet		TomoNet1		ReconNet	
Error type	AVG	STD	AVG	STD	AVG	STD	AVG	STD	AVG	STD
PSNR	21.5835	3.4374	23.0994	1.8045	32.1394	4.4240	34.5345	4.8039	31.2619	4.2749
SSIM	0.8233	0.0798	0.8727	0.0344	0.9860	0.0073	0.9911	0.0055	0.9903	0.0054
MSE	0.0091	0.0064	0.0053	0.0021	0.0010	0.0009	0.0006	0.0008	0.0012	0.0013

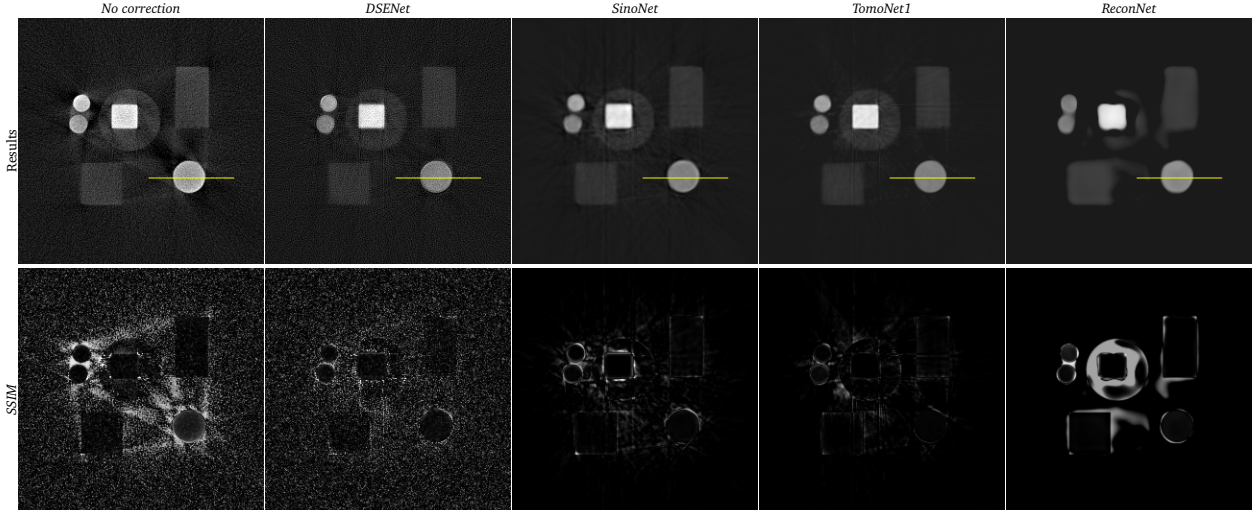


Figure 5: An example of the resulted reconstructions of the neural networks with SSIM error maps. SSIM maps are inverted for better visibility, therefore darker pixel means better result in the given location.

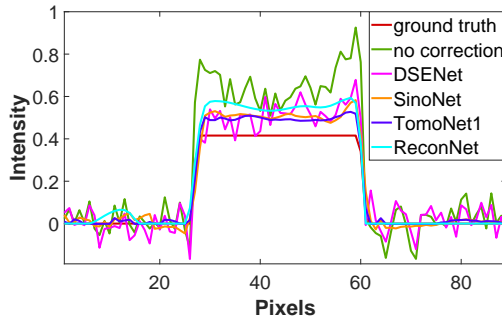


Figure 6: Intensity value profiles along the lines shown in Figure 5.

between the parts of the neural network that allowed the projection data and the reconstructed image to be improved together.

Table 2 shows the average and standard deviation values of the reconstructed phantoms produced by the tested methods. Comparing to the basic *FBP*, all of the networks improved the quality of the reconstructed images. We can also say that the *TomoNet2* outperformed the others, but it was followed closely by *TomoNet3*.

Figure 7 presents an examples from our test phantoms. The *FBP* reconstruction shows strong signs of beam hardening artifacts and electrical noise with the *FBP*. The errors have been highlighted by the Mean Absolute Error (*MAE*) error maps. The usage of *ReconNet* lead to highly homogeneous objects, but *ReconNet* did not preserve the shapes of the objects. *SinoNet* and *TomoNet1* kept the edges well, but they also left a significant amount

of artifacts on the images. *TomoNet2* and *TomoNet3* gave the best looking results. Note that *TomoNet2* resulted in more homogeneous objects, which is preferable according to the ground truth image.

Table 2: Results of the neural networks in Section 3.2

Method	FBP		SinoNet		ReconNet		TomoNet1		TomoNet2		TomoNet3	
Error type	Average	SD	Average	SD	Average	SD	Average	SD	Average	SD	Average	SD
PSNR	27.5021	4.6894	31.9951	4.3509	33.0133	4.7227	33.9611	4.5637	38.1958	4.7906	36.4728	5.2715
SSIM	0.9372	0.0399	0.9865	0.0070	0.9935	0.0041	0.9897	0.0051	0.9977	0.0016	0.9972	0.0018
MSE	0.0032	0.0042	0.0010	0.0009	0.0009	0.0013	0.0007	0.0008	0.0003	0.0004	0.0005	0.0007

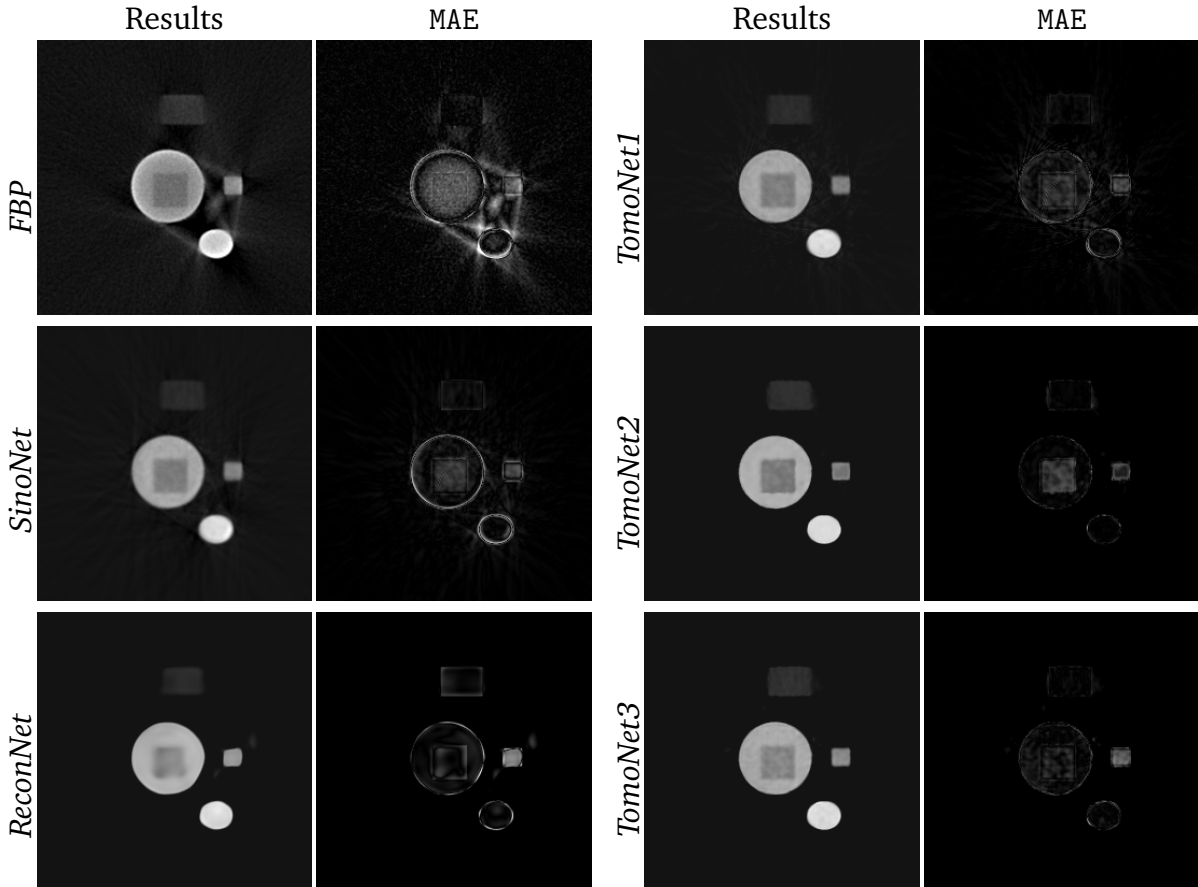


Figure 7: An example from the resulted reconstructions of Dataset A with MAE error maps.

4 Contributions of the thesis

In the **first thesis group**, the contributions are related to the errors of discrete projection geometries with different interpolation methods. I examined interpolation methods in various settings to find their advantages and disadvantages. I proved the connection between pixel coverage and the interpolation errors and showed how to reduce the effects of interpolation errors using the pixel coverage. Detailed discussion can be found in Chapter 2.

- I/1. I implemented a framework to test popular interpolation methods in various settings. The framework considers different projection geometries, seven noise levels, and two reconstruction algorithms. I evaluated the results of multiple tests on our datasets and popular head phantoms based on three error metrics.
- I/2. I found that the iterative reconstruction algorithm was less sensitive to the applied interpolation method than the analytical reconstruction algorithm.
- I/3. I proved the connection between pixel coverage and the interpolation error by experiments. I applied the pixel coverage to get a better understanding of the interpolation errors and also to visualize the different artifact structures caused by the different interpolation methods.
- I/4. I used a correction formula for the projection matrix based on pixel coverage to eliminate interpolation errors from the reconstructed images and I proved by experiments that the proposed correction method can reduce the interpolation error.
- I/5. I showed that the interpolation error of the methods can be reduced by increasing the number of projection lines, but the increased number of view angles resulted in only minor changes.

In the **second thesis group**, the contributions are related to the fusion of computed tomography algorithms and deep convolutional neural networks. The neural networks used are based on the well-known U-net architecture. The combined algorithms were compared on the basis of their noise and artifact reducing capabilities. Detailed discussion can be found in Chapter 3.

- II/1. I created a physically correct database using GATE simulation software for training and testing the neural networks. The focus of the created database was the cupping and streak artifacts caused by beam hardening and the coexisting electrical noise.
- II/2. I modified the original U-net and applied it at different stages of the image processing pipeline of computer tomography. I proposed a CNN structure (*TomoNet1*) where the reconstruction step was attached to the pre-processing CNN as a non-trainable layer. I showed by experiments that the proposed method yielded superior results in the comparison.
- II/3. I proposed two neural network architectures (*TomoNet2* and *TomoNet3*), where the reconstruction step is used as a non-trainable neural network layer in the form of skip connections. I tested the algorithms on two datasets and showed that the new architectures outperformed the others, where there was no or only one reconstruction layer inside the network.

Table 3 summarizes the relation between the thesis points and the corresponding publications.

Table 3: Correspondence between the thesis points and my publications.

Publication	Thesis point							
	I/1	I/2	I/3	I/4	I/5	II/1	II/2	II/3
[1]	•	•						
[2]		•	•	•	•			
[3]						•	•	
[4] Accepted for publication						•		•

The author's publications on the subjects of the thesis

Journal publications

- [1] **Cs. Olasz**, L. G. Varga and A. Nagy. Novel U-net based deep neural networks for transmission tomography. *Journal of X-Ray Science and Technology*, VOL(30), 13-31, 2022.

Full papers in conference proceedings

- [2] **Cs. Olasz**, L. G. Varga and A. Nagy. Evaluation of the Interpolation Errors of Tomographic Projection Models. In *14th International Symposium on Visual Computing*, Springer International Publishing, 394-406, 2019.
- [3] **Cs. Olasz**, L. G. Varga and A. Nagy. Beam hardening artifact removal by the fusion of FBP and deep neural networks. In *Thirteenth International Conference on Digital Image Processing*, SPIE, 1187817, 2021.
- [4] **Cs. Olasz** Addressing discretization artifacts in tomography by accessing and balancing pixel coverage of projections. (**Accepted**) In *International Workshop on Combinatorial Image Analysis*, Springer International Publishing, 2024.

Further related publications

- [5] **Cs. Olasz**, L. G. Varga and A. Nagy. CT scanner calibration based on optimization. In *5th Winter School of PhD Students in Informatics and Mathematics.*, 2018.
- [6] **Cs. Olasz**, L. G. Varga and A. Nagy. Tomográfiai modellek interpolációs hibájának vizsgálata. In *Képfeldolgozók és Alakfelismerők társaságának 13. konferenciája.*, 2021.

Other References

- [7] Alessandro Foi, Mejdi Trimeche, Vladimir Katkovnik, and Karen Egiazarian. Practical poissonian-gaussian noise modeling and fitting for single-image raw-data. *IEEE Transactions on Image Processing*, 17(10):1737–1754, 2008.
- [8] Gabor T. Herman. *Fundamentals of Computerized Tomography: Image Reconstruction from Projections*. Springer Publishing Company, Incorporated, 2nd edition, 2009.
- [9] Jiang Hsieh. *Computed Tomography: Principles, Design, Artifacts, and Recent Advances*. Press Monographs. SPIE, 2015.
- [10] Armando Luis Imhof, Carlos Adolfo Calvo, and Juan Carlos Santamarina. Seismic data inversion by cross-hole tomography using geometrically uniform spatial coverage. *Revista Brasileira de Geofísica*, 28(1):79–88, Jan 2010.
- [11] S Jan and et al. Gate: a simulation toolkit for pet and spect. *Physics in Medicine & Biology*, 49(19):4543, sep 2004.
- [12] S Jan and et al. Gate v6: a major enhancement of the gate simulation platform enabling modelling of ct and radiotherapy. *Physics in Medicine & Biology*, 56(4):881, jan 2011.
- [13] Avinash C. Kak and Malcolm Slaney. *Principles of Computerized Tomographic Imaging*. Society for Industrial and Applied Mathematics, 2001.
- [14] S. Krimmel, J. Baumann, Z. Kiss, A. Kuba, A. Nagy, and J. Stephan. Discrete tomography for reconstruction from limited view angles in non-destructive testing. *Electronic Notes in Discrete Mathematics*, 20:455–474, 2005. Proceedings of the Workshop on Discrete Tomography and its Applications.
- [15] Attila Kuba, Gabor Herman, Samuel Matej, and Andrew Todd-Pokropek. Medical applications of discrete tomography, discrete mathematical problems with medical applications. *DIMACS Series in Discrete Mathematics and Theoretical Computer Science*, AMS, 55:195–208, 01 2000.
- [16] Yann LeCun, Y. Bengio, and Geoffrey Hinton. Deep learning. *Nature*, 521:436–44, 05 2015.
- [17] Olaf Ronneberger, Philipp Fischer, and Thomas Brox. U-net: Convolutional networks for biomedical image segmentation. In Nassir Navab, Joachim Hornegger, William M. Wells, and Alejandro F. Frangi, editors, *Medical Image Computing and Computer-Assisted Intervention – MICCAI 2015*, pages 234–241, Cham, 2015. Springer International Publishing.
- [18] Jürgen Schmidhuber. Deep learning in neural networks: An overview. *Neural Networks*, 61:85–117, 2015.
- [19] Zhou Wang, A.C. Bovik, H.R. Sheikh, and E.P. Simoncelli. Image quality assessment: from error visibility to structural similarity. *IEEE Transactions on Image Processing*, 13(4):600–612, 2004.

5 Összefoglalás

Jelen doktori disszertáció a szerző kutatói tevékenységét mutatja be a transzmissziós számítógépes tomográfia területén. Az elvégzett kutatások célja az volt, hogy a rekonstruált képek minőségét javítsam meglévő módszerek fejlesztésével, illetve új technikák kidolgozásával.

A disszertáció két fő részből áll. A 2. Fejezet az interpolációs hibák elemzésével foglalkoztam, amelyek a vetületi adatok és a rekonstruált kép diszkrét reprezentációjából ered. A 3. Fejezetben a számítógépes tomográfia és konvolúciós neurális hálózatokat egyedi módon kombináltam a rekonstruált kép minőségének javítására sugárkeményedéssel és elektromos zajjal nagy mértékben terhelt vetületi adatok esetén.

Diszkrétizációs műtermékek

A vetületek és detektor elemek száma korlátozott egy CT berendezésben. Továbbá, a rekonstrukciót általában diszkrét rácson hajtják végre. A modell ezen megszorításai műtermékeket okoznak a rekonstruált képeken. A 2. Fejezetben bemutatom, hogy a visszavetítés során használt különböző interpolációs módszerek nagy mértékben befolyásolják ezen műtermékeket (más néven *interpolációs hibákat*). Megfigyeltem, hogy kapcsolat van a pixelek lefedettsége és az interpolációs hiba között, amely segítette az interpolációs hibák jobb megértését. Javasoltam egy módszert az interpolációs hibák hatásának csökkentésére a rekonstruált képeken. A módszert egy átfogó kísérletben megvizsgáltam, amelyben azt találtam, hogy a javasolt módszer képes szignifikánsan javítani a képek minőségét. Megfigyeltem továbbá hogy a vetítő sugarak számának növelése a vetületi geometriában képes az interpolációs hibákat csökkenteni, de a vetületi irányok számának növelése nem tudta elérni ugyanazt a szintű javulást.

Műtermékek csökkentése U-net alapú neurális hálózatokkal

A mély tanulás módszereinek használata a számítógépes tomográfiában egy hatékony mód a rekonstruált képek minőségének javítására. A 3. Fejezetben három új módszert mutatok be a sugárkeményedéssel és elektromos zajjal terhelt vetületek rekonstrukciójának javítása érdekében. A javasolt új módszerek esetén a rekonstrukciós lépés a konvolúciós neurális hálózaton belül helyezkedik el. Két neurális hálózat esetén, számos residuális kapcsolat lehetővé tette, hogy a módszerek a vetületeket és a rekonstruált képet is tudják együttesen javítani. A módszereket olyan adathalmazokon vizsgáltam, amelyeket fizikailag korrekt módon szimuláltam. Az adatokat nagy mértékű elektromos zaj és sugárkeményedés jeleit mutatják. Az objektív kiértékelést három hiba mérték segítségével végeztem a rekonstruált képeken. A kísérletek alapján a rekonstrukciós lépés alkalmazása a neurális hálózat végén vagy residuális kapcsolatokként javította a rekonstruált kép minőségét.

Nyilatkozat

Olasz Csaba "Artifact Reduction in Computed Tomography" című PhD disszertációjában a következő eredményekben Olasz Csaba hozzájárulása volt a meghatározó:

1. A disszertáció 2. fejezetében felhasznált, [1] publikációkban megjelent kutatás esetén: kísérletek tervezése, lebonyolítása és eredmények elemzése.
2. A disszertáció 3. fejezetében felhasznált, [2,3] publikációkban megjelent kutatás esetén: fantomok generálása, neurális hálók tervezése, tanítása, és eredmények kiértékelése.

Ezek az eredmények Olasz Csaba PhD disszertációján kívül más tudományos fokozat megszerzésére nem használhatók fel.



Olasz Csaba
jelölt

Dátum: 2024.01.24.



Dr. Varga László Gábor
témavezető

Dátum: 2024.01.25



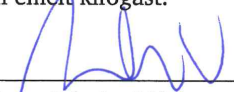
Dr. Nagy Antal
témavezető

Dátum: 2024.01.26.

Az Informatika Doktori Iskola vezetője kijelenti, hogy jelen nyilatkozatot minden társszerzőhöz eljuttatta, és azzal szemben egyetlen társszerző sem emelt kifogást.

Dátum:




Jelasity Márk
DI vezető

Hivatkozások

- [1] Cs. Olasz, L. G. Varga and A. Nagy. Evaluation of the Interpolation Errors of Tomographic Projection Models. In *Advances in Visual Computing*, Springer International Publishing, 394-406, 2019.
- [2] Cs. Olasz, L. G. Varga and A. Nagy. Beam hardening artifact removal by the fusion of FBP and deep neural networks. In *Thirteenth International Conference on Digital Image Processing*, SPIE, 1187817, 2021.
- [3] Cs. Olasz, L. G. Varga and A. Nagy. Novel U-net based deep neural networks for transmission tomography. *Journal of X-Ray Science and Technology*, VOL(30), 13-31, 2022.

